INTERNATIONAL SOCIETY FOR SOIL MECHANICS AND GEOTECHNICAL ENGINEERING



This paper was downloaded from the Online Library of the International Society for Soil Mechanics and Geotechnical Engineering (ISSMGE). The library is available here:

https://www.issmge.org/publications/online-library

This is an open-access database that archives thousands of papers published under the Auspices of the ISSMGE and maintained by the Innovation and Development Committee of ISSMGE.

The paper was published in the proceedings of the 20th International Conference on Soil Mechanics and Geotechnical Engineering and was edited by Mizanur Rahman and Mark Jaksa. The conference was held from May 1st to May 5th 2022 in Sydney, Australia.

The response of granite residual soil to high strain-rate impact loading

La réponse du sol résiduel granitique à une charge d'impact à taux de déformation élevé

Xianwei Zhang, Lingwei Kong & Cheng Chen

State Key Laboratory of Geomechanics and Geotechnical Engineering, Institute of Rock and Soil Mechanics, Chinese Academy of Sciences, Wuhan 430071, China

Xinyu Liu & Gang Wang

University of Chinese Academy of Sciences, Beijing 100049, China

ABSTRACT: The weathering process and parent rock properties generally show obvious effects on the mechanical properties of granite residual soil. Many engineering constructions on this soil are associated with the issue of soil behavior under high strain rates. Although such an issue has been well studied for sedimentary soils, little is known about the response of granite residual soil under impact loading with high strain rate. This paper explores the mechanical behavior of granite residual soil under high strain rates via split-Hopkinson pressure bar tests. The responses of soil under strain rates up to 255.22 s⁻¹ were obtained. The residual soil under the studied range of strain rate generally show strain-softening behavior, and the peak strength and axial strain at failure are found to increase with strain rates. However, the dependency of peak strength on strain rates varies at different ranges of the strain rate, and a coefficient of strain-rate sensitivity is proposed for the quantitative evaluation of such dependency. The sensitivity under a low strain rate is more obvious, and the obtained coefficient is found to be exceedingly higher than that under high strain rates. Despite the strength increase, impact loading has been proven to be harmful, as damage of soil structure especially in terms of degrading cementation and extending fissures occur on soil samples under such condition. This research enhances the understanding of how residual soil responds under high strain rates and serves as a guide for related engineering issues.

RÉSUMÉ: Le processus d'altération et les propriétés de la roche mère montrent généralement des effets évidents sur les propriétés mécaniques du sol granitique résiduel. De nombreuses constructions techniques sur ce sol sont associées à la question du comportement du sol sous des taux de déformation élevés. Bien qu'une telle question ait été bien étudiée pour les sols sédimentaires, on en sait peu sur la réponse du sol granitique résiduel sous une charge d'impact avec un taux de déformation élevé. Cet article explore le comportement mécanique du sol granitique résiduel sous des taux de déformation élevés via des tests de barre de pression Split-Hopkinson. Les réponses du sol à des taux de déformation jusqu'à 255,22 s⁻¹ ont été obtenues. Le sol résiduel dans la plage étudiée de taux de déformation montre généralement un comportement de ramollissement de la déformation, et la résistance maximale et la déformation axiale à la rupture augmentent avec les taux de déformation. Cependant, la dépendance de la résistance maximale aux taux de déformation varie à différentes plages de la vitesse de déformation, et un coefficient de sensibilité à la vitesse de déformation est proposé pour l'évaluation quantitative de cette dépendance. La sensibilité sous un faible taux de déformation est plus évidente, et le coefficient obtenu s'avère être excessivement plus élevé que celui sous des taux de déformation élevés. Malgré l'augmentation de la résistance, la charge d'impact s'est avérée nocive, car des dommages à la structure du sol, en particulier en termes de dégradation de la cimentation et d'extension des fissures, se produisent sur les échantillons de sol dans de telles conditions. Cette recherche permet de mieux comprendre comment le sol résiduel réagit à des taux de déformation élevés et sert de guide pour les problèmes d'ingénierie connexes.

KEYWORDS: Granite residual soil, strain rate, impact loading, cementation, fissures.

1 INTRODUCTION

Granite residual soil (GRS) is widely known to exhibit different mechanical behaviors from sedimentary soil mainly due to the structure features as a result of its parent rock (decomposed granite) and weathering process. The structure features show a dual effect on soil strength, namely (i) the cementation among soil particles greatly enhance soil strength, and (ii) the fissures formed during weathering process reduces soil strength. The unique structure of residual soil has brought challenges in predicting its mechanical behavior. With the development of civil engineering works on residual soils worldwide in recent years, the mechanical behavior of GRS under static and conventional cyclic loading has been thoroughly investigated (Lumb 1965; Lee & Coop 1995). However, the above research failed to consider the effect of the high strain rate. Granite residual soil is frequently subjected to impact loading with a high strain rate, especially when engineering practices such as blasting and dynamic compaction occurs on residual soil. These loads are distinct from traditional dynamic loading with a strain rate higher than 10 s⁻¹. In contrast, the strain rate for conventional static

loading typically falls within the range of 10^{-7} to 10^{-4} s⁻¹. Hence, the response of soil to impact loading may well differ from that to conventional loadings.

Currently, the effect of impact loading on residual soil is far from established, despite wide recognition of its effect on sedimentary soils (Bragov et al. 1994; Martin et al. 2013). However, the studies on sedimentary soils are inapplicable to residual soil because of its the unique formation history and structural characteristics (Zhang et al. 2020). The impact loading may well damage the cementation and extend the fissures in residual soil, which may cause strength degradation and large deformation. Thus, it is critical to investigate the response of residual soil under impact loading.

In this study, a series of split Hopkinson pressure bar (SHPB) tests were performed on natural granite residual soil under different strain rates up to 255.22 s⁻¹. Briefer comments were also given on the soil behavior within the domain of low strain rate through unconfined compressive strength test. This paper firstly detailed of the soil characteristics and test procedure. Then, the stress-strain behavior and strength properties were presented, where the effect of the strain rate is highlighted. Finally, a quantitative evaluation of the effect of strain rate was

given. This paper enhances the understanding of the mechanic response of granite residual soil and decomposed rocks in general.

2 MATERIALS AND METHOD

2.1 Characteristics of granite residual soil

Undisturbed soil blocks (30 cm in width and 30 cm in height) were retrieved at a foundation pit in Xiamen Island, at southeastern China. The sampling depth was around 10.0 m. Some important index properties of the GRS were summarized in Table 1. From this table, it can be found that the studied residual soil is sandy clay composed of 12.5% gravel, 36.3% sand, and 51.2% clay (ASTM D 2487-17, 2017). The residual soil was deposited in saturated condition, which is distinctive from many unsaturated residual soils in tropical regions (Futai & Almeida, 2005) due to the high underground water level (1.5 m). The effective shear strength parameters were also obtained from CIU tests. The high friction angle of studied soil is typical of granite-originated residual soil, which is partially due to the quartz in soil. The presence of quartz leads to more frictional contacts among particles. X-ray diffraction analysis confirmed

the high content of quartz (42.6%). Note that hematite with a content of 3.2% was also detected, which was proved to enhance the soil strength by forming cementation in the structure of soil (Zhang et al. 2017). Some micro-level investigations given by Liu. et al. (2019) found the iron-bearing cementation in this soil was sensitive to disturbance and may decay under impact loading. Besides, their study also revealed that the fissure was one of the dominant structural features, which would extend and develop under impact loading.

2.2 Test apparatus

A split Hopkinson pressure bar (SHPB) testing system (Figure 1) was adopted, which is capable of applying impact loading with strain rate ranged between 10 s⁻¹ to 10000 s⁻¹. One of the important features of this apparatus is the ability to collect faint transmission signals with the help of the semiconductor strain gauges, which is an effective method when investigating the materials with a low wave impedance. A waveform shaper was also attached to the end of the incident bar to facilitate a stress equilibrium as well as reduce wave dispersion (Song & Chen 2005).

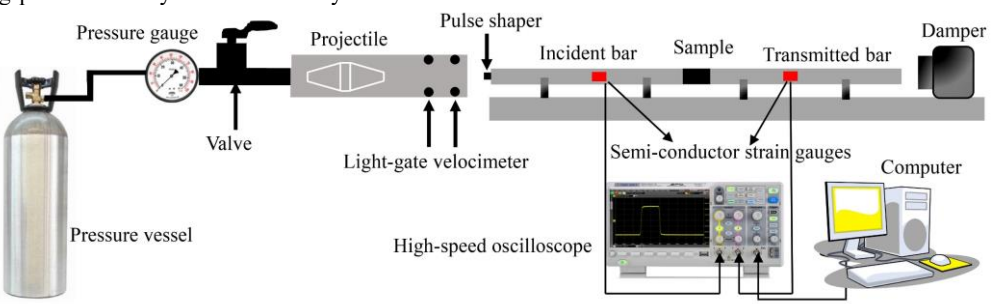


Figure 1. Shematic of adopted SHPB apparatus

Table 1. Average basic indices of granite residual soil

Phisical indices Density ρ (g/cm³) Specific gravity G_s Vater content w (%) Liquid limit w_L (%) Plastic limit w_p (%) Plasticity index I_p Quartz (%) Kaolinite (%) Mica (%) Feldspar (%) Shear strength parameters Effective cohesion c' (kPa) Effective friction angle w' (°) 1.82 2.72 4.8 48.1 2.72 48.1 8.1 Effective friction angle w' (°) 32.13	Index	Value
Specific gravity G_s 2.72 Water content w (%) 34.6 Liquid limit w_L (%) 48.1 Plastic limit w_p (%) 24.8 Plasticity index I_p 23.3 Mineralogy Quartz (%) 42.6 Kaolinite (%) 38.9 Mica (%) 9.6 Feldspar (%) 5.6 Hematite (%) 3.3 Shear strength parameters Effective cohesion c' (kPa) 8.1	Phisical indices	
Water content w (%) 34.6 Liquid limit w_L (%) 48.1 Plastic limit w_p (%) 24.8 Plasticity index I_p 23.3 Mineralogy 42.6 Kaolinite (%) 38.9 Mica (%) 9.6 Feldspar (%) 5.6 Hematite (%) 3.3 Shear strength parameters Effective cohesion c' (kPa) 8.1	Density ρ (g/cm ³)	1.82
Liquid limit w_L (%)48.1Plastic limit w_p (%)24.8Plasticity index I_p 23.3Mineralogy23.3Quartz (%)42.6Kaolinite (%)38.9Mica (%)9.6Feldspar (%)5.6Hematite (%)3.3Shear strength parametersEffective cohesion c' (kPa)8.1	Specific gravity $G_{\rm s}$	2.72
Plastic limit w_p (%) 24.8 Plasticity index I_p 23.3 Mineralogy Quartz (%) 42.6 Kaolinite (%) 38.9 Mica (%) 9.6 Feldspar (%) 5.6 Hematite (%) 33.3 Shear strength parameters Effective cohesion c' (kPa) 8.1	Water content w (%)	34.6
Plasticity index I_p 23.3 Mineralogy Quartz (%) 42.6 Kaolinite (%) 38.9 Mica (%) 9.6 Feldspar (%) 5.6 Hematite (%) 3.3 Shear strength parameters Effective cohesion c' (kPa) 8.1	Liquid limit w_L (%)	48.1
Mineralogy Quartz (%) 42.6 Kaolinite (%) 38.9 Mica (%) 9.6 Feldspar (%) 5.6 Hematite (%) 3.3 Shear strength parameters Effective cohesion c' (kPa) 8.1	Plastic limit w_p (%)	24.8
Quartz (%) 42.6 Kaolinite (%) 38.9 Mica (%) 9.6 Feldspar (%) 5.6 Hematite (%) 3.3 Shear strength parameters Effective cohesion c' (kPa) 8.1	Plasticity index I_p	23.3
Kaolinite (%) 38.9 Mica (%) 9.6 Feldspar (%) 5.6 Hematite (%) 3.3 Shear strength parameters Effective cohesion c' (kPa) 8.1	Mineralogy	
Mica (%) 9.6 Feldspar (%) 5.6 Hematite (%) 3.3 Shear strength parameters Effective cohesion c' (kPa) 8.1	Quartz (%)	42.6
Feldspar (%) 5.6 Hematite (%) 3.3 Shear strength parameters Effective cohesion c' (kPa) 8.1	Kaolinite (%)	38.9
Hematite (%) 3.3 Shear strength parameters Effective cohesion c' (kPa) 8.1	Mica (%)	9.6
Shear strength parameters Effective cohesion c' (kPa) 8.1	Feldspar (%)	5.6
Effective cohesion c' (kPa) 8.1	Hematite (%)	3.3
* /	Shear strength parameters	
Effective friction angle $\varphi'(\circ)$ 32.13	Effective cohesion c' (kPa)	8.1
	Effective friction angle φ' (°)	32.13

2.3 *Test scheme and procedure*

Table 2 presented the test schemes. S0 in Table 2 represented a trial test without a specimen to ensure the coaxiality of the bars. S1 to S6 represented specimens for SHPB tests under the strain rate ranging from 34.68 to 255.22 s⁻¹. Several unconfined compressive strength tests were performed (sample U1 to U4) on the samples with identical dimension according to ASTM standard, making comparisons with samples tested under high strain rates.

The hand-trimmed samples with a diameter of 100 mm and a height of 50 mm were prepared, with Vaseline applied on their ends to reduce friction. After adjusting the air pressure and opening pneumatic valves (Figure 1), the bullet was driven by the air pressure and shocked the incident bar and consequently the impact test was initiated. The signals of the incident wave,

reflected wave, and transmitted wave were simultaneously recorded by the strain gauges mounted on incident and transmission bars. The data interpretation was shown in Eq. 1 (Wang & Shang 2014).

$$\sigma(t) = \frac{E_0 A_0}{A_S} \varepsilon_T(t)$$

$$\varepsilon(t) = \frac{C_0}{I_S} \int_0^t \left[\varepsilon_1(t) - \varepsilon_R(t) - \varepsilon_T(t) \right] dt$$

$$\dot{\varepsilon} = \frac{C_0}{I_S} \left[\varepsilon_1(t) - \varepsilon_R(t) - \varepsilon_T(t) \right]$$

$$C_0 = \sqrt{\frac{E_0}{\rho_0}}$$
(1)

Where $\varepsilon_{\rm I}(t)$, $\varepsilon_{\rm R}(t)$, and $\varepsilon_{\rm T}(t)$ are the incident, reflected, and transmitted strain, respectively. The meaning and value of other symbols are detailed in Table 3. The calculated strain rates $\dot{\varepsilon}$ and corresponding impact air pressures are listed in Table 2.

Table 2. Test schemes

Sample	Air Pressure (MPa)	Bullet Velocity (m·s ⁻¹)	$\dot{\varepsilon}$ (s ⁻¹)
U1	_	-	1.67×10 ⁻⁴
U2	_	_	5×10^{-4}
U3	_	_	8.3×10^{-4}
U4	_	_	1.67×10^{-3}
S0	0.1	5.303	-
S1	0.05	3.221	34.68
S2	0.093	5.102	99.45
S3	0.136	6.356	175.27
S4	0.177	7.060	255.22
S5	0.211	8.84	-
S6	0.243	9.66	-

The typical obtained waveforms were displayed in Figure 2, which proves the reliability of the tests. It should be noted that when the impact loading pressure was relatively high, the specimen was damaged instantly and distinct nonuniform deformation occurred (sample S5 and S6, as will be shown later in Figure 5), which indicated that the stress equilibrium can be barely reached and the calculated strain rate as well as the stress-strain curves may be erroneous. Thus, the test results in this condition were not applicable for quantitative investigations while the failure modes of these specimens were qualitatively analyzed.

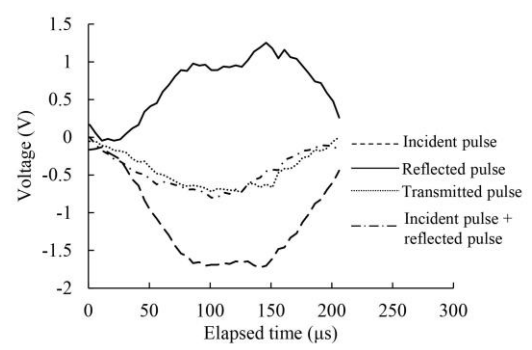


Figure 2. Typical incident, reflected and transmitted wave form

Table 3 Parameters of bars

Parameters	Value
Length of bar l_s (m)	2.5
Young's modulus E_0 (GPa)	200
Cross area ratio A_0/A_S	1
Wave velocity C_0 (m·s ⁻¹)	5172.19
Density of bars ρ (kg·m ⁻³)	7850

3 TEST RESULTS AND ANALYSIS

The general stress-strain behavior of granite residual soil under different strain rates range was depicted in Figure 3. The photographs showing the damage characteristics of each specimen are shown in Figure 4 and 5. From Figure 3, it can be found that granite residual soil showed a strain softening response under different strain rates, although the peak value for axial stress obtained under high strain rates was not as welldefined as that at low strain rates. The studied residual soil under low strain rate showed obvious strain softening behavior [Figure 3(a)] with the occurrence of fissures and shear bands (Figure 4). Well-defined peak values for axial stress were observed when axial strain ε_a is around 3.0%, as shown in Figure 3(a). Since then, soil displayed a significant decrease in strength, and axial stress σ generally was below 10 kPa when ε_a exceeded 7.5%. A less obvious strain-softening feature under high strain rate was observed [see for example Sample S1 in Figure 3(b)] which was consistent with the less-developed shear bands, minor fissures and small soil fragments were generated (Figure 5).

Figure 3 also indicated the effect of strain rate on the strength properties of residual soil. With the increasing of strain rate, the affected region of specimen seemed to be expanded and soil was damaged to larger fragments (Figure 5, Sample S5 and S6). This phenomenon agreed with the increasingly obvious strain softening behavior as indicated by the stress-strain curves in Figure 3(b). Besides, the axial strain corresponding to the peak value of axial stress ε_{af} increased with strain rate, and the increment was more apparent under high strain rates.

The strength of the soil, expressed as the peak value for axial stress σ_{max} , was generally higher under high strain rates [Figure 3(c)]. The σ - ε_a curves moved upward as the strain rate increased and the relationship between peak strength σ_{max} and strain rate could be fitted using Eq. 2 [Figure 3(c)].

$$\sigma_{\text{max}} = \begin{cases} 26.69 \, \dot{\varepsilon} + 0.20, \text{ low strain rates }, R^2 = 0.95 \\ 0.01 \, \dot{\varepsilon} + 0.29, \text{ high strain rates }, R^2 = 0.98 \end{cases}$$
 (2)

The increment of strength can be explained as follows. Due to the instantaneity nature of impact loading, specimens under higher strain rate had less sufficient time to form a shear band. In addition, soil particle rearrangement occurred under high-speed impact loading leading to an improvement of friction angle. Similar conclusions have also been drawn by Zhang, et al (2019).

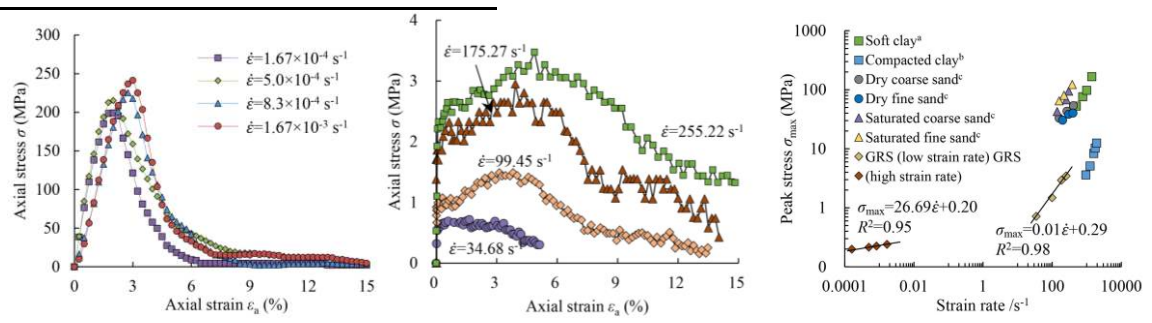


Figure 3. Test results for intact granite residual soil. (a) Stress-strain curves obtained under high strain rate. (b) Stress-strain curves obtained under low strain rate. (c) The variation of peak strength of GRS with strain rate. Data source: a–Bragov et al. 1994; b–Leroueil & Hight 2003; c–Xia et al. 2015.

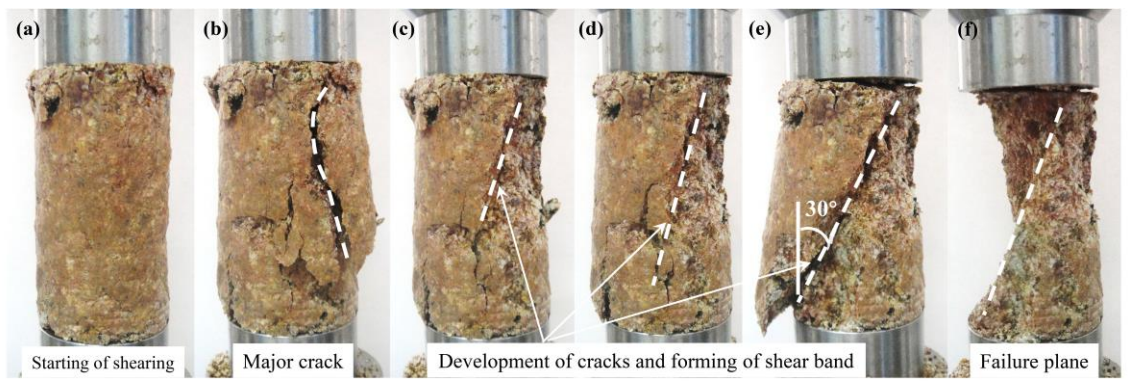


Figure 4. Failure process of granite residual soil in unconfined compressive test

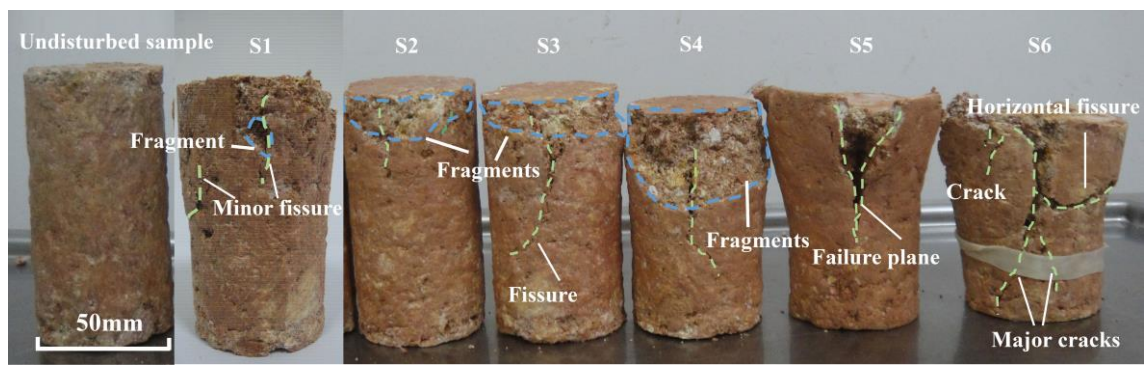


Figure 5 Photographs of specimens at failure under high strain rate

Interestingly, within different $\dot{\varepsilon}$ ranges, the residual soil seems to show different degrees of sensitivity to strain, as reflected by the different inclination of fitting curves in Figure 3(b). More specifically, when the strain rate showed a tenfold improvement increasing from $1.67 \times 10^{-4} \, \mathrm{s^{-1}}$ to $1.67 \times 10^{-3} \, \mathrm{s^{-1}}$, the σ_{\max} of the specimen was increased by 21.25%. When $\dot{\varepsilon}$ increased from 175.27 s⁻¹ to 255.22 s⁻¹, σ_{\max} raised rapidly only by 16.1%, implying a declining sensitivity of σ_{\max} to strain rate. It is therefore important to quantitatively evaluate the effect of strain rate on granite residual soil. The coefficient of sensitivity to strain rate m is proposed herein to evaluate the dependence of the strength on the strain rate, as defined in Eq. 3.

$$m = \frac{\Delta \sigma_{\text{max}}}{\Delta \varepsilon} \tag{3}$$

Where $\Delta \dot{\varepsilon}$ and $\Delta \sigma_{\rm max}$ represented the incremental value of the strain rate and the induced variation of peak strength, respectively. From Eq. 3 it was clear that when soil has a higher value of m, its strength showed a higher degree of strain-rate dependency.

Table 4. The value of m of various soils

Soils	Maximum strain rate (s ⁻¹)	m (MPa·s)
Granite residual soil	1.67×10 ⁻³	26.69
Granite residual soil	255.22	0.01
Soft clay ^a	1400	0.13
Compacted clay ^b	1932	0.01
Dry sand ^c	410	0.08
Saturated sand ^c	380	0.30

Data source: a–Bragov et al. 1994; b–Leroueil & Hight 2003; c–Xia et al. 2015.

The m values from different types of soil were summarized in Table 4. It can be found that the m value for granite residual soil in this paper under high strain rates was close to that of fine-grained soil and compacted clay but quite distinct from that of

sand. More specifically, m reached 26.69 MPa·s and 0.01 MPa·s, respectively, under low and high strain rates, implying a decrease in sensitivity of σ_{max} to strain rate as $\dot{\varepsilon}$ increased. It can be seen from the photos of specimens at failure (Figure 5) that as the strain rate increased, the affected region in specimen expanded. In particular, fracture surfaces and horizontal fissures throughout specimens S5 and S6 can be observed, which may lead to the degradation of soil strength. Consequently, the impact loading with high strain rate is overall harmful to soil despite strength increase. When soil is impacted under high strain rate, the cementation of soil gradually degrades and the fissures in soil extend, which may lead to the damage of soil structure hence the declining of strain rate sensitivity of soil strength. It is reasonable to expect that a strain rate higher than that in this paper may lead to strength degradation, which is consistent with the strain-rate softening features of soil (Di Prisco et al. 2000).

4 CONCLUSIONS

This study focuses on the effect of high strain-rate impact loading on the strength properties of granite residual soil through a series of SHPB tests and unconfined compressive tests. The main conclusions are as follows:

- (i) Under low strain rate, the stress-strain curves of residual soil show obvious strain softening with a well-defined peak value. With the occurrence of the shear band, soil displays a significant decrease in strength, and axial stress σ generally is below 10 kPa when ε_a exceeds 7.5%. The stress-strain behavior of granite residual soil under high strain rates is similar to that under low strain rate, except less obvious strain-softening.
- (ii) The peak strength of the soil is generally higher under high strain rates. The σ-εa curves move upward as the strain rate increases and the relationship between peak strength σ_{max} and strain rate could be fitted by linearly relations.
- (iii) A new parameter *m* was proposed to quantitatively evaluate the sensitivity to strain rate. The value of *m* reached 26.69

- MPa·s and 0.01 MPa·s under low and high strain rates respectively, indicating a decreasing sensitivity of soil strength to strain rate.
- (iv) Despite the increasing strength under high strain rate, impact loading is overall harmful to residual soil as such load may damage of soil structure especially in terms of degrading cementation and extending fissures.

5 ACKOWLEDGEMENTS

The authors gratefully acknowledge the financial support of the National Natural Science Foundation of China (Nos. 41972285, 41672293 and 51709290), the Youth Innovation Promotion Association CAS (Grant No. 2018363), the opening fund of State Key Laboratory of Geohazard Prevention and Geoenvironment Protection (Grant No. SKLGP2020K024) and Science Fund for Distinguished Young Scholars of Hubei Province (2020CFA103).

6 REFERENCES

- ASTM D 2487–17. 2017. Standard practice for classification of soils for engineering purposes (unified soil classification system). Annual Book of ASTM Standards, American Society for Testing and Materials, West Conshohocken, PA.
- Bragov, A.M., Grushevsky, G.M., and Lomunov, A.K. 1994. Use of the Kolsky method for studying shear resistance of soils. *Dymat Journal* 3(1), 253-259.
- Futai, M.M., and Almeida, M.S.S. 2005. An experimental investigation of the mechanical behaviour of an unsaturated gneiss residual soil. *Géotechnique* 55(3), 201-213.
- Lee, I.K., and Coop, M.R. 1995. The intrinsic behaviour of a decomposed granite soil. *Géotechnique* 45(1), 117-130.
- Leroueil, S., and Hight, D.W. 2003. Characterisation and engineering properties of natural soils, *proceedings of the international workshop*, pp 29-254, Singapire.
- Liu, X.Y., Zhang, X.W., Kong, L.W., and Xu, C. 2019. Structural damage and dynamic failure mechanism of granite residual soils under impact loading. *Chinese Journal of Geotechnical Engineering* 41(10), 1872-1881. (in Chinese)
- P. Lumb. 1965. The residual soils of Hong Kong. Géotechnique 15(2), 180-194.
- Di Prisco, C., Imposimato, S., and Vardoulakis, I. 2000. Mechanical modelling of drained creep triaxial tests on loose sand. Géotechnique 50(1), 73-82.
- Song, B., and Chen, W. 2005. Split Hopkinson pressure bar techniques for characterizing soft materials. *Latin American Journal of Solids* and Structures 2, 113-152.
- Wang, T.T., and Shang, B. 2014. Three-Wave Mutual-Checking Method for Data Processing of SHPB Experiments of Concrete. *Journal of Mechanics* 30(05), 5-10.
- Xia, K.W., Jafari, M., Kanopoulos, P.P., and Wei, Y. 2015. Constitutive Modelling of Soils under High Strain Rates. Toronto: University of Toronto.
- Zhang, X.W., Kong, L.W., Yin, S., and Chen, C. 2017. Engineering geology of basaltic residual soil in Leiqiong, southern China. *Engineering Geology* 220(2017), 196-207.
- Zhang, X.W., Liu, X.Y., Kong, L.W., and Xu, C. 2019. Experimental study on mechanical characteristics of granite residual soil under blast loading. *Scientia Sinica Technologica* 49(6), 690-702 (in Chinese).
- Zhang, X.W., Liu, X.Y., Chen, C., Kong, L.W., and Wang, G. 2020. Engineering geology of residual soil derived from mudstone in Zimbabwe. *Engineering Geology* 277(2020), 1-11.